TDA Progress Report 42-105

May 15, 1991

Elevation Control System Model for the DSS 13 Antenna

W. Gawronski and J.A. Mellstrom
Ground Antennas and Facilities Engineering Section

In order to meet the requirements for precision pointing of 34-m antennas, adequate control design and simulation software have to be developed, with a detailed description of the supporting analytical tools. This article describes a control system model for the elevation drive of the DSS 13 antenna. The model allows one to simulate elevation dynamics, cross-coupled dynamics in azimuth and elevation, and RF pointing error. A modal state-space model of the antenna structure was obtained from its finite-element model with a free rotating tipping structure. Model reduction techniques were applied separately for the antenna model and rate-loop model, thereby reducing the system order to one-third of the original one while preserving its dynamic properties. Extensive simulation results illustrate properties of the model.

I. Introduction

In order to meet the requirements for the 34-m antenna pointing accuracy, an appropriate control system model has to be developed. The purpose of this article is to give a detailed description of the antenna control system modeling. This analytical approach is the background for the computer software development, which is used for the simulations of antenna dynamics due to control input, disturbances, and parameter variations, and is a tool for the control system design.

A state-space control system model for elevation pointing of the DSS 13 antenna is described. Special attention is paid to antenna structure modeling. A finite-element model of the antenna structure with a free rotating tipping structure is used to obtain its state-space model in modal coordinates. The model was developed with the following assumptions:

(1) Linearity of the model (nonlinear effects due to dry friction are omitted).

(2) The structural model consists of mode shapes up to 5 Hz.

(3) The elevation angle of the tipping structure is 90 deg.

(4) The azimuth rotation joint is locked.

(5) No disturbances act on the structure.

The balanced reduction technique was applied to reduce the structural model and subsequently the rate-loop model. The order of the resulting reduced model is one-third of the original one, while the modeling error is insignificantly small. Extensive simulations were performed and are described below to illustrate the control system properties.[1]

[1] W. Gawronski, "Software Package for Modeling and Simulation of the Elevation Control System for the DSS 13 Antenna," JPL Interoffice Memorandum 3324-91-016 (internal document), Jet Propulsion Laboratory, Pasadena, California, February 6, 1991.

II. Structural Model

Here and throughout the article, the state-space representation of a system is used. This representation is denoted by a triple (A, B, C), which represents a first-order differential equation in the form

$$\dot{x} = Ax + Bu, \qquad y = Cx \tag{1}$$

Assuming the state vector x of dimension $n \times 1$, the input u of dimension $p \times 1$, and the output y of dimension $q \times 1$, the matrices A, B, and C are of dimensions $n \times n$, $n \times p$, and $q \times n$, respectively.

The state-space model for an antenna structure with a 90-deg elevation angle and locked azimuth rotation is obtained. A balanced reduction technique applied to the structural model gives the smallest acceptable model.

A. Full Model

In this section the state-space triple (A_s, B_s, C_s) for the antenna structure is determined. The triple is obtained in modal coordinates. The state vector of the structure x_s consists of modal displacements q_s and modal velocities v_s:

$$x_s^T = [q_s^T, \; v_s^T] \tag{2}$$

The antenna structural model is generated from the natural frequencies ω_i and mode shapes ϕ_i, obtained from the finite-element model generated by JPL/IDEAS, and presented in Appendix A. Modal damping of the structure ζ_i is assumed to be 0.5 percent, i.e., $\zeta_i = 0.005$ for $i = 1, \ldots, 10$. The antenna is a free rotating structure with a joint between the alidade and tipping structure. Hence, the open-loop structural model is unstable. From the finite-element model, $m = 10$ modes are obtained; the first one is the rigid-body mode with zero natural frequency. The modes are determined for selected p points of interest. Thus, $\phi_i = [\phi_{i1}, \phi_{i2}, \ldots, \phi_{ip}]^T$ for $i = 1, \ldots, 10$.

1. Matrix A_s. Denote

$$\Omega = diag(\omega_i), \quad Z = diag(\zeta_i), \quad i = 1, 2, \ldots, m \tag{3}$$

Then, the system matrix A_s for the antenna structure is

$$A_s = \begin{bmatrix} 0 & I_m \\ -\Omega^2 & -2Z\Omega \end{bmatrix} \tag{4}$$

where I_m is the identity matrix of dimensions $m \times m$. Details of the derivation of A_s are presented in Appendix B. The numerical values of Ω, Z, and other parameters are given in Appendix A.

2. Matrix B_s. The bull-gear–pinion connection is shown in Fig. 1. The rollers of the connection are redundant; they compensate for gravity forces. The rigid pinion housing includes two drive systems. A torque applied at the pinion of the gearbox is the input to the structure. The pinion radius is $r_p = 6$ inches. A node labeled $no = 86302$ in the finite-element model is a point of contact between the pinion and the bull gear, while a node with the label $nu = 86881$ is located at the joint of the supporting truss structure and the pinion housing. The joint nu is at distance ρ from node no. The distance ρ is small in comparison to the bull gear radius; thus, in further analysis the nodes nu and no coincide. The torque T applied to the pinion is in equilibrium with tangential (to the bull gear and the pinion) forces F_{no} and F_{nu}, see Fig. 2. For the force F_{no} with y and z components F_{noy} and F_{noz}, and the absolute value $|F_{no}|$, one obtains from Fig. 2

$$|F_{no}| = |T|/r_p,$$

$$F_{noy} = |F_{no}| \sin\alpha, \quad F_{noz} = |F_{no}| \cos\alpha$$

Hence,

$$F_{no} = \begin{bmatrix} F_{noy} \\ F_{noz} \end{bmatrix} = \begin{bmatrix} r_p^{-1} \sin\alpha \\ r_p^{-1} \cos\alpha \end{bmatrix} T = B_{no} T$$

where $B_{no} = r_p^{-1}[\sin\alpha \;\; \cos\alpha]^T$ and $\alpha = 28$ deg. From Fig. 2, one can see that $F_{nu} = -F_{no}$; hence, $F_{nu} = -B_{no}T$. In global coordinates, the force F_s acting on the structure is a vector $F_s^T = [0 \;\; 0 \;\cdots\; F_{no}^T \;\; 0 \;\cdots\; F_{nu}^T \;\; 0 \;\cdots\; 0]$. Thus,

$$F_s = B_o T$$

where $B_o^T = [0 \;\; 0 \;\cdots\; B_{no}^T \;\; 0 \;\cdots\; -B_{no}^T \;\; 0 \;\cdots\; 0]$. The matrix B_o is transformed into modal coordinates:

$$B_s = M_m^{-1} \Phi^T B_o \tag{5a}$$

where $M_m = diag(m_{m1}, \ldots, m_{mm})$ is the modal mass matrix. Denoting $\phi_{no} = [\phi_{1no}, \ldots, \phi_{mno}]$, $\phi_{nu} = [\phi_{1nu}, \ldots,$

$\phi_{mnu}]$, $\phi_{ino}^T = [\phi_{inoy}\ \phi_{inoz}]$, and $\phi_{inu} = [\phi_{inuy}\ \phi_{inuz}]$, where ϕ_{inoy} is the ith mode component at node no, at y direction (mode shapes are listed in Appendix A), the above equation reduces to

$$B_s = M_m^{-1}(\Phi_{no} - \Phi_{nu})B_{no} \tag{5b}$$

3. Matrix C_s. The following outputs of the antenna structure are considered: elevation angle θ_e, elevation rate $\dot{\theta}_e$, pinion rate $\dot{\theta}$, pointing error angle in the x direction ε_x, and pointing error angle in the y direction ε_y. Hence, the antenna output matrix C_s consists of five rows: C_{s1} for the elevation angle, C_{s2} for the elevation rate, C_{s3} for the pinion rate, C_{s4} for pointing error in the x direction, and C_{s5} for pointing error in the y direction:

$$C_s^T = [C_{s1}^T\ C_{s2}^T\ C_{s3}^T\ C_{s4}^T\ C_{s5}^T] \tag{6}$$

The first two rows of C_s are determined as follows. In the finite-element model, the node at the bull gear center has a label $nb = 5380$, and the node at distance R to nb has a label $nc = 41212$ (see Fig. 2). High stiffness of the bull gear and the close location of the two nodes allows one to determine the elevation angle as a rigid-body rotation:

$$\theta_e = (y_{nc} - y_{nb})/R$$

$$= (C_{ncy}\Phi - C_{nby}\Phi)x_s/R = (\phi_{ncy} - \phi_{nby})x_s/R$$

where C_{ncy} and C_{nby} denote rows with all but one zero elements. The nonzero element of C_{ncy} is equal to 1, and is located in the position corresponding to the location of y displacement at node nc in the vector x_s. The nonzero element of C_{nby} is equal to 1, and located in the position corresponding to the location of y displacement at node nb in the vector x_s. Furthermore, $\phi_{ncy} = [\phi_{1ncy}, \ldots, \phi_{mncy}]$, where ϕ_{incy} is the ith mode component at node nc at y direction, and $\phi_{nby} = [\phi_{1nby}, \ldots, \phi_{mnby}]$, where ϕ_{inby} is the ith mode component at node nb at y direction. From the above, it follows that

$$C_{s1} = [0\ C_{se}], \qquad C_{s2} = [C_{se}\ \ 0] \tag{7a}$$

where $C_{se} = (\phi_{ncy} - \phi_{nby})/R$.

For the determination of the pinion rate measurement matrix C_{s3}, denote the velocity at pinion housing v_p (at node nu), bull gear velocity v_b at node no (see Fig. 2), and their y and z components by v_{py}, v_{pz}, v_{by}, and v_{bz}, respectively. Projections of v_b and v_p onto directions tangential to the bull gear at node no are denoted v_1 and v_2, respectively.

$$v_1 = v_{by}\sin\alpha + v_{bz}\cos\alpha, \quad v_2 = v_{py}\sin\alpha + v_{pz}\cos\alpha$$

The pinion rate is $\dot{\theta} = (v_1 - v_2)/r_p$, and noting that $v_{by} = \phi_{noy}v_s$, $v_{bz} = \phi_{noz}v_s$, $v_{py} = \phi_{nuy}v_s$, and $v_{pz} = \phi_{nuz}v_s$, where v_s is a modal velocity defined in Eq. (2), one obtains

$$v_1 - v_2 = [(\phi_{noz} - \phi_{nuz})\cos\alpha + (\phi_{noy} - \phi_{nuy})\sin\alpha]v_s$$

Therefore, $\dot{\theta} = C_{sp}v_s = [0\ \ C_{sp}]x_s$, giving finally

$$C_{s3} = [0\ \ C_{sp}] \tag{7b}$$

where $C_{sp} = [(\phi_{noz} - \phi_{nuz})\cos\alpha + (\phi_{noy} - \phi_{nuy})\sin\alpha]/r_p$.

The last two rows of C_s, the output matrices for the pointing error in the x and y directions, are:

$$C_{s4} = [C_{ex}\ \ 0], \qquad C_{s5} = [C_{ey}\ \ 0] \tag{7c}$$

where C_{ex} = [333.26, 0.07973, −0.60701, 0.15431, 48.635, 4.0901, −40.343, 113.24, 225.17, −39.59] and C_{ey} = [−9.0557, −24.706, −6.6233, 3.6844, −19.179, 23.571, 43.871, 180.87, −59.909, −227.56] are obtained from the JPL/IDEAS.

B. Model Reduction

The structural model under consideration consists of 10 modes or 20 states. The set of modes may consist of modes which are not important in system dynamics and can thus be eliminated. Observability and controllability properties are used to determine which modes to eliminate. Observability is a property of a system that indicates the participation of each system state in the output with all states equally excited. Controllability, on the other hand, indicates the excitation of each state due to white noise, or impulse input. A balanced representation [1] is a state-space representation with its states equally controllable and observable, and the Hankel singular value is the measure of the joint controllability and observability of each balanced state variable. The states with small Hankel singular values can be deleted, since they are weakly excited and weakly observed at the same time, causing minimal

modeling error. For flexible structures, modal representation is almost balanced, assuming small damping and distinct poles [2,3]. Each mode has almost the same controllability and observability property, hence, each mode can be considered for reduction separately. The Hankel singular value for the ith mode is given by Eq. (53) of [2] and Eq. (14) of [4]:

$$\gamma_i = \frac{\overline{(b_{si}b_{si}^T)(c_{si}^T c_{si})}}{4\zeta_i\omega_i^2} \tag{8}$$

where b_{si} is the ith row of B_s and c_{si} is the ith column of C_s. For the rigid-body mode, the Hankel singular value does not exist—its value tends to infinity—hence, the rigid-body mode is always included in the reduced model. For each mode, the Hankel singular value is determined to help the designer decide on the number of modes in the reduced structural model.

Hankel singular values of the 10-mode model of the antenna (A_s, B_s, C_s) are plotted in Fig. 3, where the Hankel singular value of the rigid-body mode is omitted. The reduced-order model consists of five modes: the rigid-body mode and four elastic modes with natural frequencies 3.1358, 4.1149, 4.4503, and 4.5688 Hz, indicated in Fig. 3. The transfer functions of the full and reduced models of the antenna are shown in Fig. 4, indicating that the reduced model fully represents properties of the original system. Note that disturbances are not included in the model; therefore, they are not considered in model reduction. One should note, however, that a different reduced model would be obtained for a model with disturbances included.

III. Rate-Loop Model

This section presents details of rate-loop modeling and introduces model reduction.

A. Full Model

The rate-loop model of the antenna is shown in Fig. 5. It consists of two identical subsystems denoted G_o, antenna structure G_s, command amplifier G_c, and the bias loop, with the bias command v_{bias}.

The subsystem G_c is shown in Fig. 6(a). The first state variable is denoted $x_1 = v_1$ and its state equation is

$$\dot{x}_i = -\tau_1^{-1}x_1 + k_1 k_s\ \tau_1^{-1}\ \dot{\theta}_o \tag{9}$$

The subsystem G_o, Fig. 6(b), consists of four subsystems itself: G_1, G_2 (both amplifiers), G_3 (motor armature), and G_4 (motor and gearbox mechanical properties). The state equations for G_1 are

$$\dot{x}_2 = x_3 \tag{10a}$$

$$\dot{x}_3 = x_1 - \tau_3^{-1}x_3 - k_{tach}x_7 \tag{10b}$$

where $x_7 = \omega_m$. Similarly, for G_2:

$$\dot{x}_4 = x_5 \tag{11a}$$

$$\dot{x}_5 = k_r\tau_3^{-1}x_2 + k_r\tau_2\tau_3^{-1}x_3 - \tau_5^{-1}x_5 - k_{cur}x_6 \tag{11b}$$

where $x_6 = i_o$. For G_3, from Fig. 6:

$$\dot{x}_6 = k_f k_i L_a^{-1}\tau_5^{-1}x_4 + k_f k_i \tau_4 L_a^{-1}\tau_5^{-1}x_5$$

$$- R_a L_a^{-1}x_6 - k_b L_a^{-1}x_7 \tag{12a}$$

$$T_o = k_m x_6 \tag{12b}$$

The system G_4 denotes the motor and gearbox model. There are two inputs to the system: motor torque T_o and pinion rate $\dot{\theta}$. The output is the pinion torque T. The gearbox flexibility is described either by the input or the output stiffness, as shown in Figs. 7(a) and 7(b). For the output stiffness model, with notations as in Fig. 7(a), one obtains equations for the gearbox rate

$$T_N = NT_o, \qquad \theta_N = \theta_m/N$$

and the dynamic equilibrium equations

$$J_m\dot{\omega}_m + T_N/N = T_o$$

along with the spring equation for the output stiffness k_{go}

$$T = T_N = k_{go}(\theta_m - N\theta)/N$$

Similar equations are derived for the input stiffness model in Fig. 7(b). Both models are represented by Fig. 8, where $N_x = 1/N$ and $k_{gx} = k_{go}$ for the output stiffness

model and $N_x = N$ and $k_{gx} = k_{gi}$ for the input stiffness model. Denoting $x_8 = T$, the state equations are

$$\dot{x}_7 = k_m J_m^{-1} x_6 - J_m^{-1} N^{-1} x_8 \tag{13a}$$

$$\dot{x}_8 = k_{gx} N_x x_7 - k_{gx} N_x N C_s x_s \tag{13b}$$

where $N_x = N$ for $k_{gx} = k_{gi}$, and $N_x = 1/N$ for $k_{gx} = k_{go}$.

Combining Eqs. (10)–(13) for models G_1, G_2, G_3, and G_4, one obtains the state-space model for G_o (inputs v_1 and $\dot{\theta}$, outputs T and i_o, and state vector $x_o = [x_2, x_3, x_4, x_5, x_6, x_7, x_8]^T$):

$$\dot{x}_o = A_1 x_0 + B_{11} v_1 + B_{12} \dot{\theta} \tag{14a}$$

$$\begin{bmatrix} T \\ i_0 \end{bmatrix} = C_1 x_o \tag{14b}$$

where

$$A_1 = \begin{bmatrix} 0 & 1 & 0 & 0 & 0 & 0 & 0 \\ 0 & -1/\tau_3 & 0 & 0 & 0 & -k_{tach} & 0 \\ 0 & 0 & 0 & 1 & 0 & 0 & 0 \\ k_r/\tau_3 & k_r\tau_2/\tau_3 & 0 & -1/\tau_5 & -k_{cur} & 0 & 0 \\ 0 & 0 & k_f k_i/L_a\tau_5 & k_f k_i \tau_4/L_a\tau_5 & -R_a/L_a & -k_b/L_a & 0 \\ 0 & 0 & 0 & 0 & k_m/J_m & 0 & -1/J_m N \\ 0 & 0 & 0 & 0 & 0 & k_{gx} N_x & 0 \end{bmatrix}$$

$$B_{11}^T = [0\ 1\ 0\ 0\ 0\ 0\ 0], \quad B_{12}^T = [0\ 0\ 0\ 0\ 0\ 0\ -k_{gx} N_x N], \quad C_{11} = [0\ 0\ 0\ 0\ 0\ 0\ 1],$$

$$C_{12} = [0\ 0\ 0\ 0\ 1\ 0\ 0], \quad C_1 = \begin{bmatrix} C_{11} \\ C_{12} \end{bmatrix}, \quad B_1 = [B_{11}\ B_{12}]$$

Two systems' G_o's are located in the rate-loop system (see Fig. 5): the first with inputs v_{11} and $\dot{\theta}$, outputs T_1 and i_{o1}, and state vector x_{21}, and the second with inputs v_{12} and $\dot{\theta}$, outputs T_2 and i_{o2}, and state vector x_{22}. The equations for these systems are

$$\dot{x}_{21} = A_1 x_{21} + B_{11} v_{11} + B_{12} \dot{\theta} \tag{15a}$$

$$\begin{bmatrix} T_1 \\ i_{01} \end{bmatrix} = C_1 x_{21} \tag{15b}$$

and

$$\dot{x}_{22} = A_1 x_{22} + B_{11} v_{12} + B_{12} \dot{\theta} \tag{16a}$$

$$\begin{bmatrix} T_2 \\ i_{o2} \end{bmatrix} = C_1 x_{22} \tag{16b}$$

The subsystem G_c is an amplifier for the bias signal, with input Δv_c and output v_u. Denoting $x_a = v_u$, its state space equation is obtained:

$$\dot{x}_a = -\tau_6^{-1} x_a + k_{ctfr} \tau_6^{-1} \Delta v_c \tag{17}$$

The antenna structure equations according to Section II are

$$\dot{x}_s = A_s x_s + B_s T, \quad \dot{\theta}_e = C_{s2} x_s, \quad \dot{\theta} = C_{s3} x_s \tag{18}$$

The nodal equations are

$$T = T_1 + T_2, \quad T_1 = C_{11}x_{21}, \quad T_2 = C_{11}x_{22} \tag{19a}$$

$$\Delta v_c = v_{c1} - v_{c2} + k_{bs}v_{bias} = k_{ct}C_{12}(x_{21} - x_{22}) + k_{bs}v_{bias} \tag{19b}$$

$$v_{11} = v_1 - v_u = x_1 - x_a, \quad v_{12} = v_1 + v_u = x_1 + x_a \tag{19c}$$

Denoting the state vector $x_r^T = [x_1^T, x_{21}^T, x_{22}^T, x_a^T, x_s^T]$ and combining Eqs. (9)–(19), the equations for the whole system can be written

$$\dot{x}_r = A_r x_r + B_r u, \quad y = C_r x_r \tag{20}$$

where $u^T = [\dot{\theta}_o \;\; v_{bias}]$ and $y^T = [\theta_e^T \;\; \dot{\theta}_e^T \;\; \dot{\theta}^T]$, and

$$A_r = \begin{bmatrix} -1/\tau_1 & 0 & 0 & 0 & 0 \\ B_{11} & A_1 & 0 & -B_{11} & B_{12}C_{s3} \\ B_{11} & 0 & A_1 & B_{11} & B_{12}C_{s3} \\ 0 & p_1 & -p_1 & -1/\tau_6 & 0 \\ 0 & B_sC_{11} & B_sC_{11} & 0 & A_s \end{bmatrix}$$

$$B_r^T = \begin{bmatrix} k_1k_s/\tau_1 & 0 & 0 & 0 & 0 \\ 0 & 0 & 0 & p_2 & 0 \end{bmatrix},$$

$$C_r = \begin{bmatrix} 0 & 0 & 0 & 0 & C_{s1} \\ 0 & 0 & 0 & 0 & C_{s2} \\ 0 & 0 & 0 & 0 & C_{s3} \end{bmatrix},$$

$$p_1 = k_{ctfr}k_{ct}C_{12}/\tau_6, \quad p_2 = k_{ctfr}k_{ct}/\tau_6$$

B. Model Reduction

The rate-loop system model is reduced by applying the balancing principle. The system is transformed into balanced coordinates where each state is equally controllable and observable and not correlated with other states. The balancing procedure from [3] is used, and is summarized in Appendix C. The procedure from Section II is applicable to flexible structures only.

The rate-loop system, with already reduced antenna structural modes, has 26 state variables. A plot of the system Hankel singular values is shown in Fig. 9. The Hankel singular values of component number 15 and larger are small in comparison to the remaining components. Therefore, the reduced system consists of 14 state variables. The transfer functions of the reduced and full rate-loop systems are compared in Fig. 10. The full system contains the full structural model: 36 state variables altogether. From Fig. 10 one can see that the reduced model of 14 state variables almost exactly approximates the full 36-state model. In Fig. 11 step responses of full and reduced models are compared, showing good agreement between the full and reduced models.

IV. Position-Loop Model

The rate-loop system, with the position loop closed, is shown in Fig. 12. A proportional-plus-integral (PI) controller is applied. For the state x_o defined $x_o^T = [x_r^T \;\; x_i]$, the state-space triple of the series connection of the rate-loop system and the controller is

$$A_o = \begin{bmatrix} A_r & B_tk_{ii} \\ 0 & 0 \end{bmatrix}, \quad B_o = \begin{bmatrix} B_tk_{pp} \\ 1 \end{bmatrix},$$

$$C_o = [C_t \;\; 0], \quad B_{ob} = \begin{bmatrix} B_{bi} \\ 0 \end{bmatrix} \tag{21}$$

where k_{pp} and k_{ii} are the proportional and integral parameters of the controller, B_t is the first column of B_r, B_{bi} is the second column of B_r, and C_t is the first row of C_r. The closed-loop system matrix is

$$A_{cl} = A_o - B_oC_o \tag{22}$$

and the closed-loop triple is (A_{cl}, B_o, C_o). The closed-loop system performance is illustrated in Fig. 13 in time domain and in Fig. 14 in frequency domain. One can see that the x component of the RF pointing error is much larger than the component in the y direction, and the y component of subreflector vertex displacement is much larger than the component in the x direction. In fact, for a symmetric

structure the RF y component and x displacement of the subreflector vertex should be zero.

Finally, the action of the bias input v_{bias} is tested. Two step inputs are introduced to the closed-loop system: a v_{bias} step of amplitude 2.5 V at the moment $t = 0$ sec and a command step θ_o of amplitude 0.1 deg at the moment $t = 10$ sec. The results are shown in Figs. 15(a) through 15(c). For the first 10 sec, when the command θ_o is zero, the torques T_1 and T_2 are equal but with opposite sign, so that the resulting torque T acting on the structure is zero: v_{bias} does not influence the structure. Nevertheless, both motors are active, their rates ω_{m1} and ω_{m2} are nonzero, plotted in Fig. 15(c). After 10 sec, when the command is active, the system behavior is similar to the one without bias.

V. Conclusions

In this article, modeling techniques for the DSS 13 antenna structure and its rate-loop control system have been presented. Through balancing the system controllability and observability properties, a reduced system model has been obtained. Antenna dynamics, rate-loop dynamics, and dynamics of a system with a closed position loop have been simulated. The model allows one to simulate elevation dynamics, cross-coupled dynamics in azimuth and elevation, and a dynamic RF pointing error.

Section I contains restrictions that need to be relaxed. The structural model could include modes of up to 10 Hz, with free elevation and azimuth joints. The elevation and azimuth control systems could be simulated jointly, exposing the cross-coupling of the two systems. Disturbances (wind and measurement noise) could be included in the model. The system could be modeled for several elevation angles of the range of [0 deg, 90 deg], and the dependence of the system dynamics on elevation angle investigated. Nonlinear effects due to dry friction and saturations could be included. Finally, field measurements need to be performed, and the model parameters adjusted such that a satisfactory agreement between simulations and field data is achieved.

Acknowledgments

The authors thank Robert Hill, Roy Levy, Ben Parvin, and Douglas Strain for their extensive and useful discussions.

References

[1] B. C. Moore, "Principal Component Analysis in Linear Systems: Controllability, Observability and Model Reduction," *IEEE Trans. Autom. Control*, vol. 26, no. 1, pp. 17–32, January 1981.

[2] W. Gawronski and J.-N. Juang, "Model Reduction for Flexible Structures," in *Control and Dynamics Systems*, ed. C. T. Leondes, vol. 36, New York: Academic Press, 1990.

[3] E. A. Jonckheere, "Principal Component Analysis of Flexible Systems—Open Loop Case," *IEEE Trans. Autom. Control*, vol. 29, no. 12, pp. 1095–1097, December 1984.

[4] W. Gawronski and T. Williams, "Model Reduction for Flexible Space Structures," *Journal of Guidance, Control, and Dynamics*, vol. 14, no. 1, pp. 68–76, January 1991.

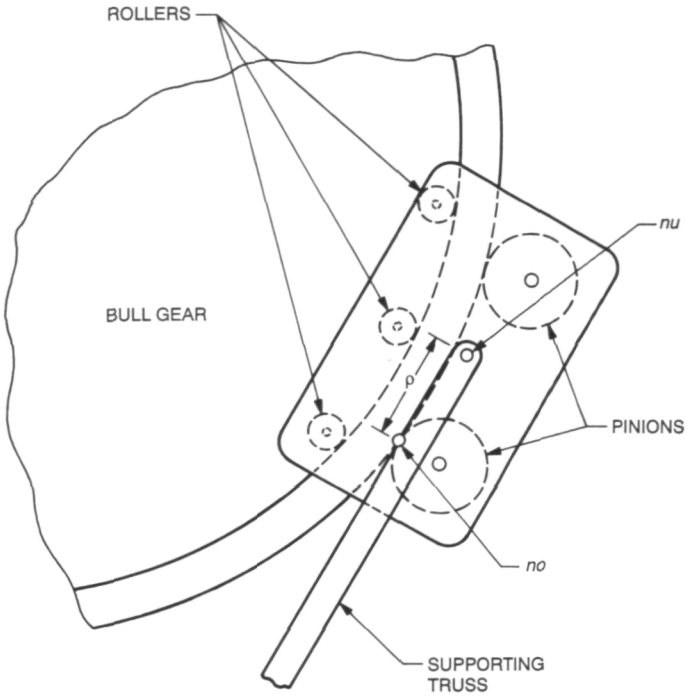

Fig. 1. Bull-gear–pinion connection.

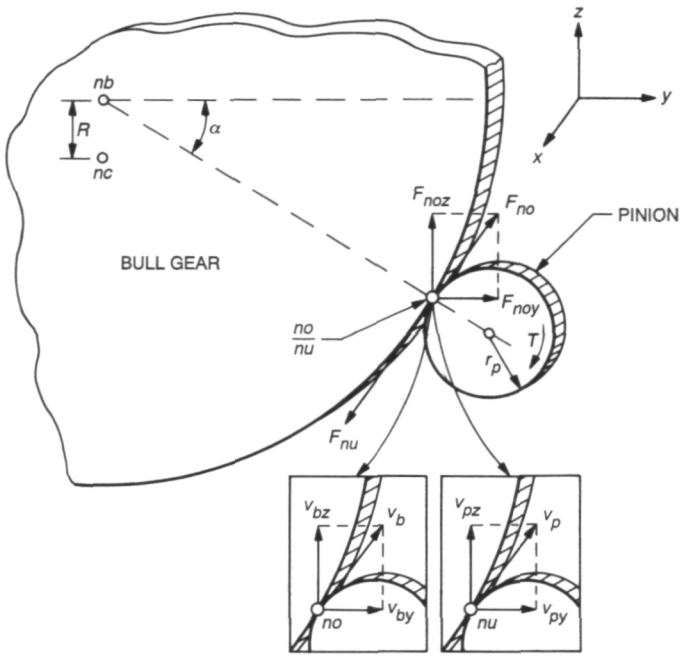

Fig. 2. Forces and velocities at the bull-gear–pinion connection.

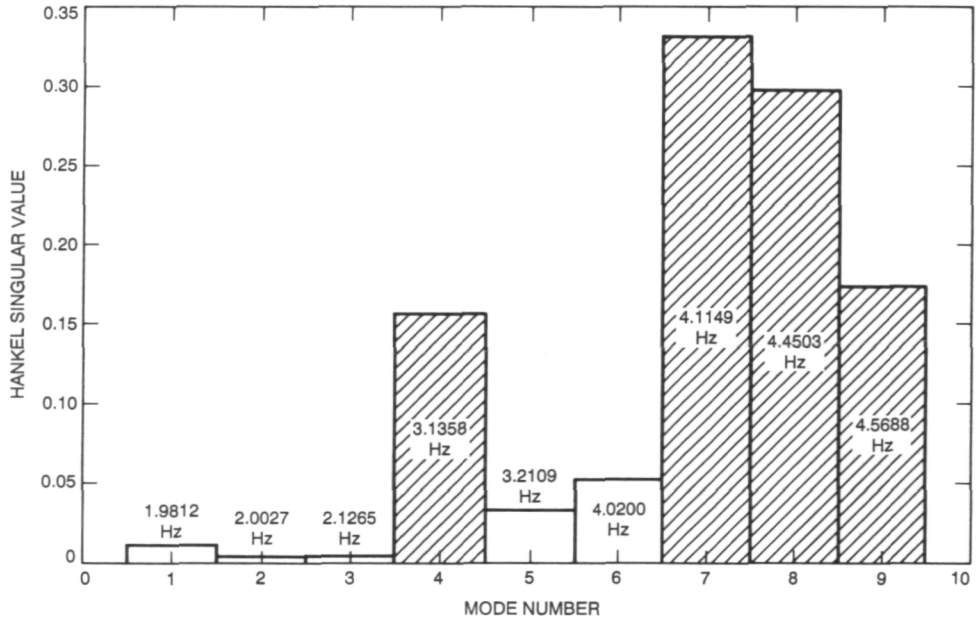

Fig. 3. Hankel singular values for the antenna structure.

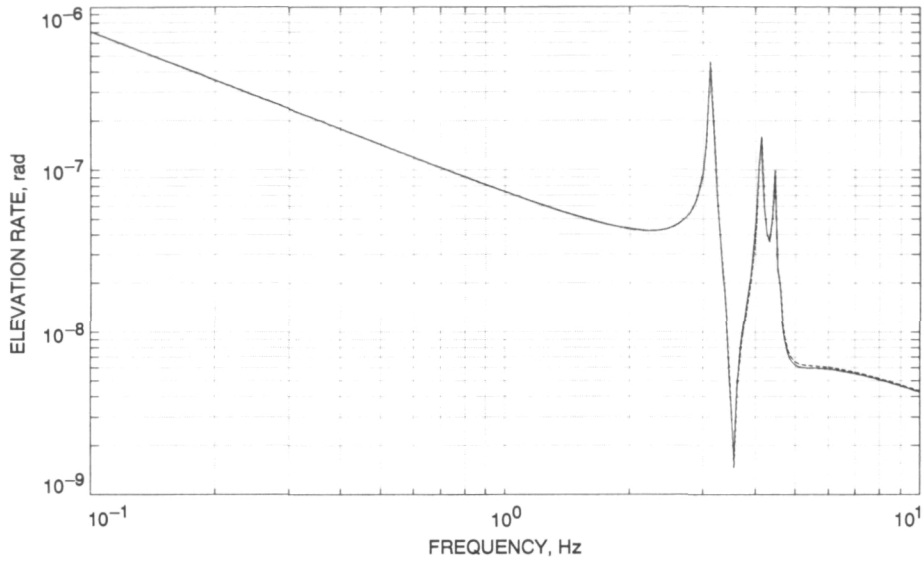

Fig. 4. Magnitude of the elevation rate transfer function for the full 10-mode (solid line) and the reduced 5-mode (dashed line) models of the antenna structure.

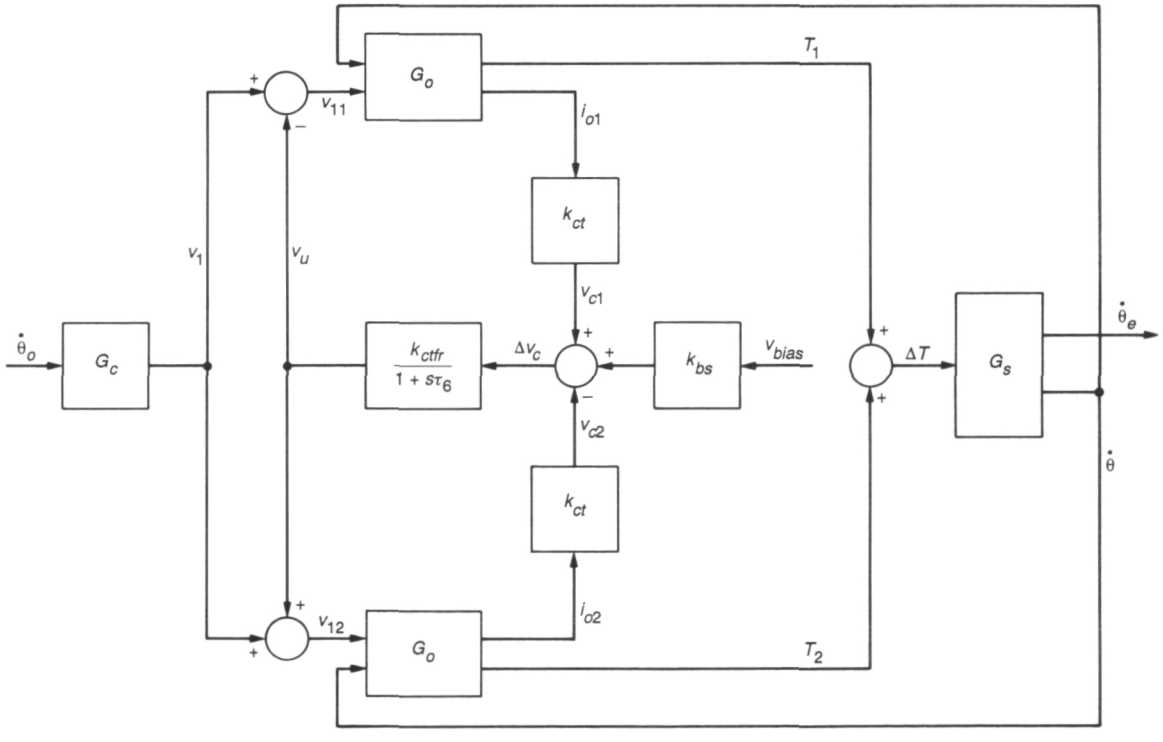

Fig. 5. Rate-loop control system.

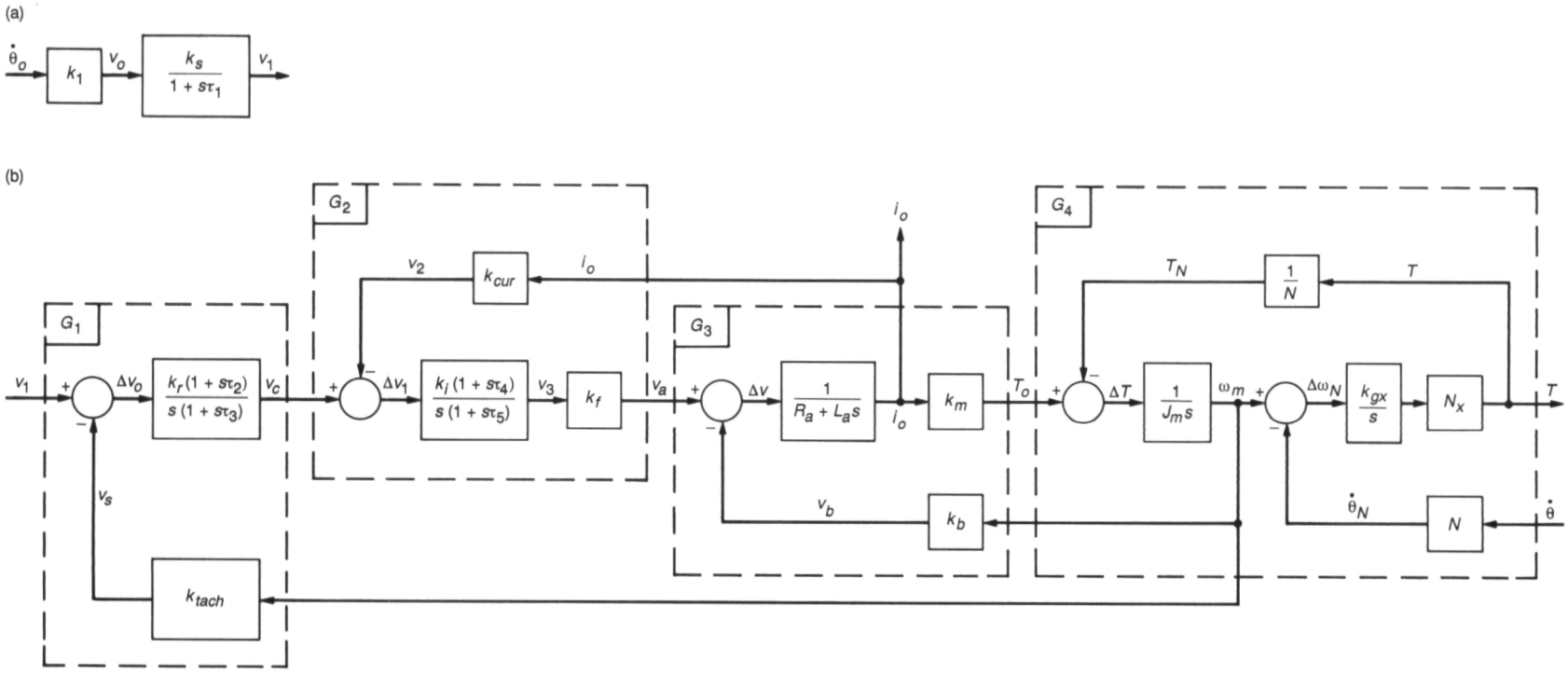

Fig. 6. Rate-loop subsystems: (a) subsystem G_c, and (b) subsystem G_o.

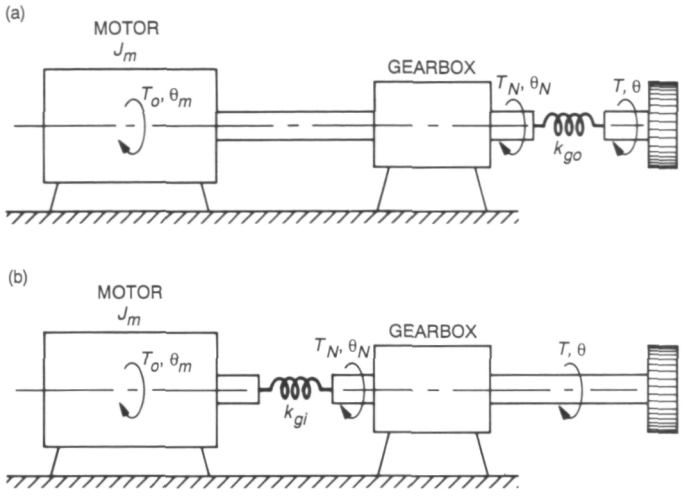

Fig. 7. Motor and gearbox configuration: (a) output stiffness model, and (b) input stiffness model.

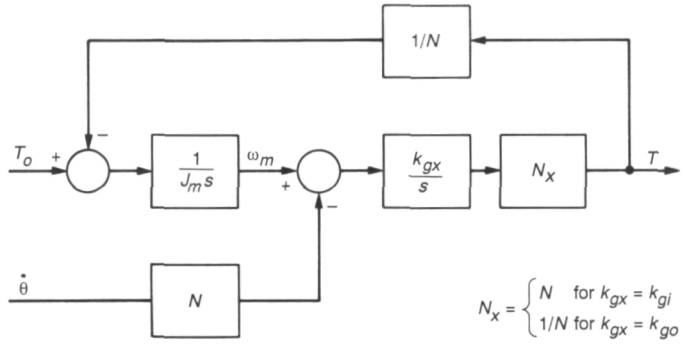

Fig. 8. Motor and gearbox model.

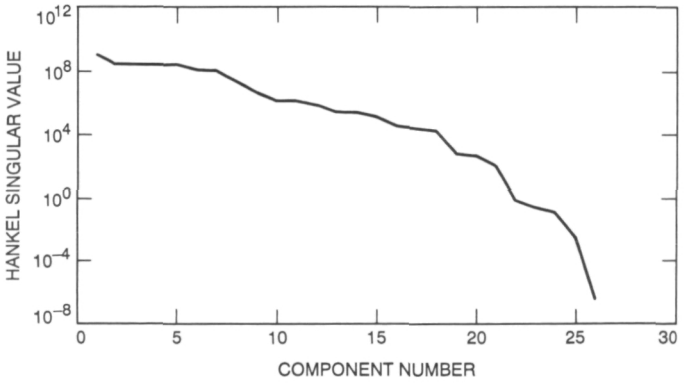

Fig. 9. Hankel singular values for the rate-loop system.

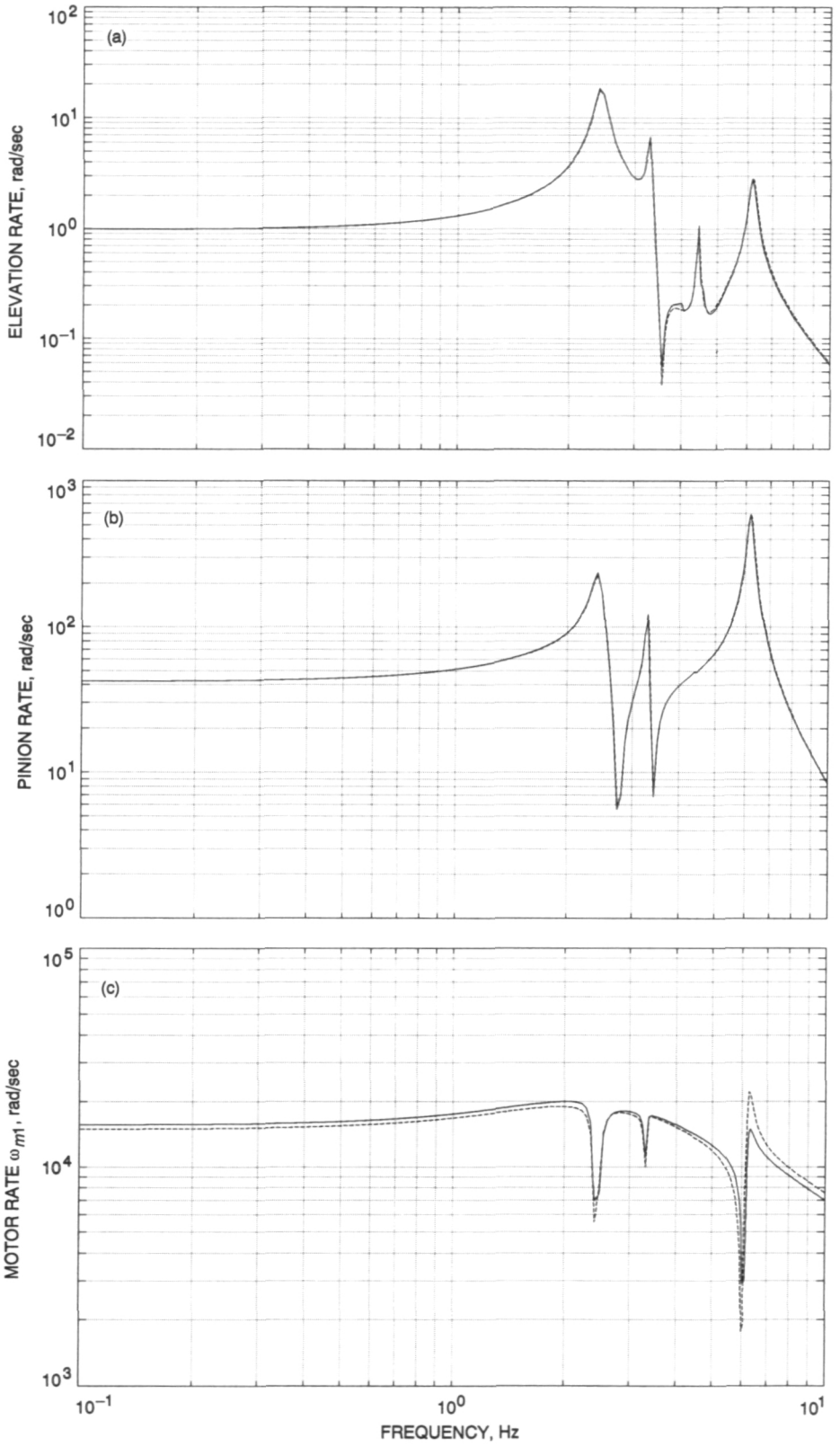

Fig. 10. Magnitudes of transfer function for the full 36-state (solid line) and the reduced 14-state (dashed line) rate-loop models (input: elevation rate, rad/sec).

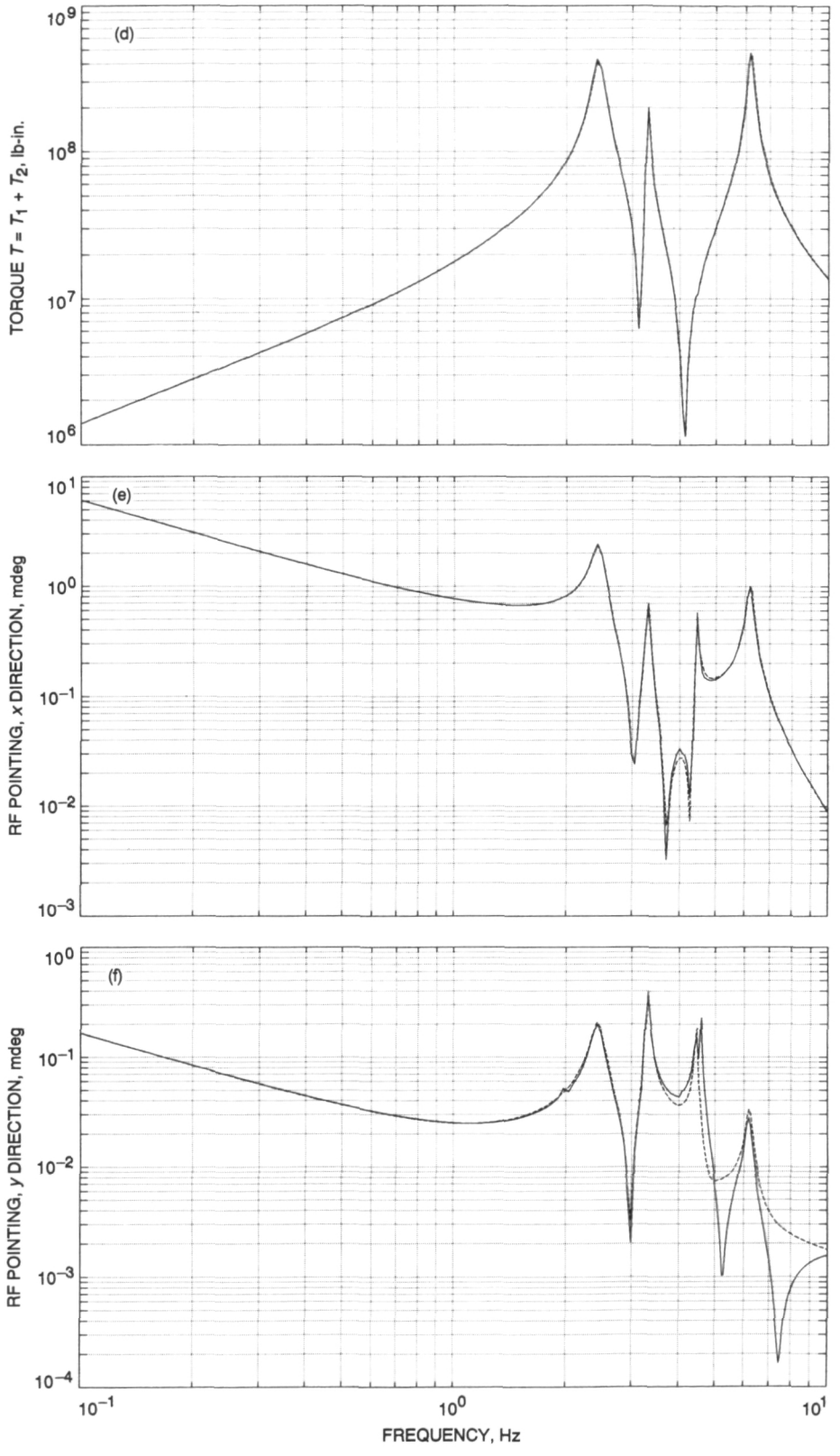
(d)
TORQUE $T = T_1 + T_2$, lb-in.
10^9
10^8
10^7
10^6
(e)
RF POINTING, x DIRECTION, mdeg
10^1
10^0
10^{-1}
10^{-2}
10^{-3}
(f)
RF POINTING, y DIRECTION, mdeg
10^0
10^{-1}
10^{-2}
10^{-3}
10^{-4}
10^{-1}
10^0
10^1
FREQUENCY, Hz

Fig. 10 (contd)

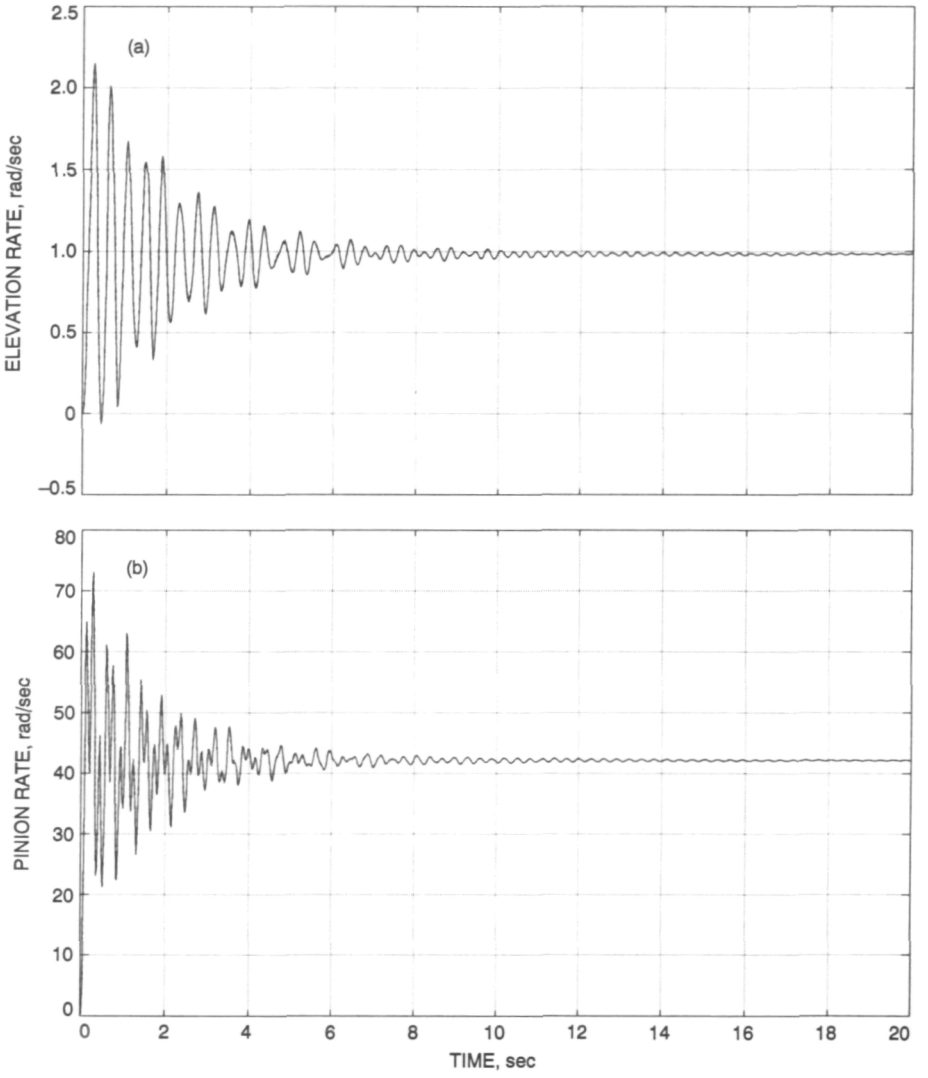

Fig. 11. Step responses of the full 36-state (solid line) and reduced 14-state (dashed line) rate-loop models (input: elevation rate, rad/sec).

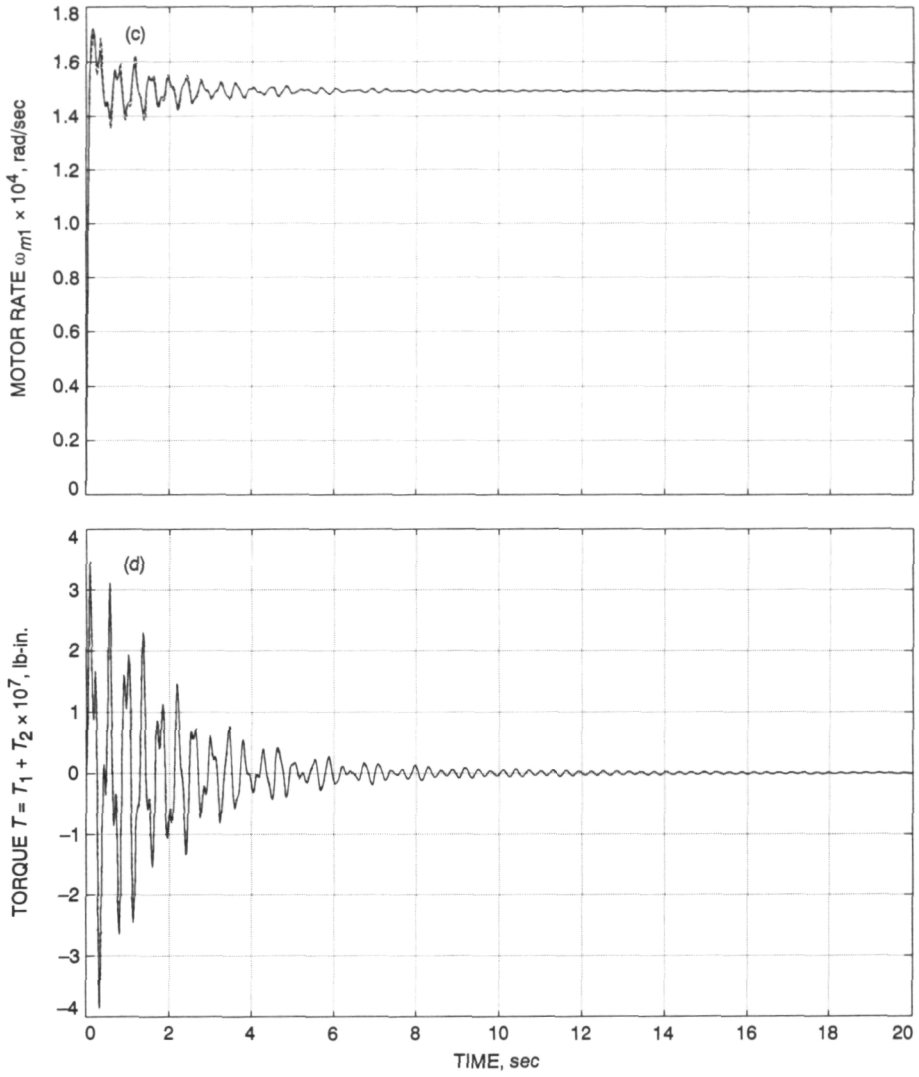

Fig. 11 (contd)

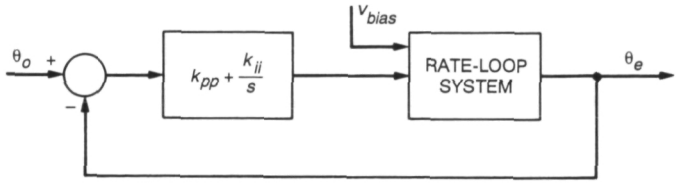

Fig. 12. Position-loop system.

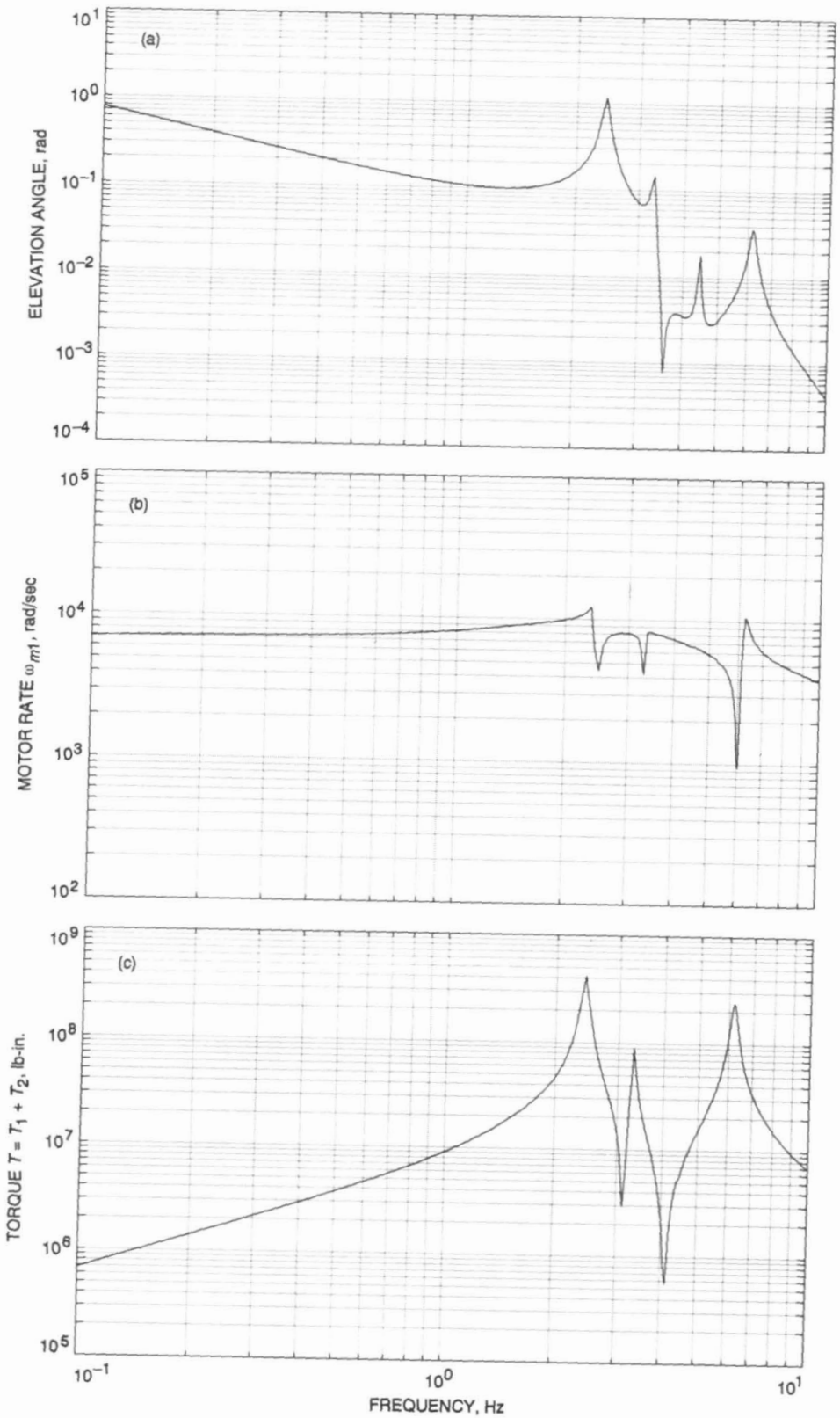

Fig. 13. Magnitudes of transfer function for the position-loop system; position loop closed, $k_{pp} = 0.5$, $k_{ii} = 0.1$; input: elevation angle, rad.

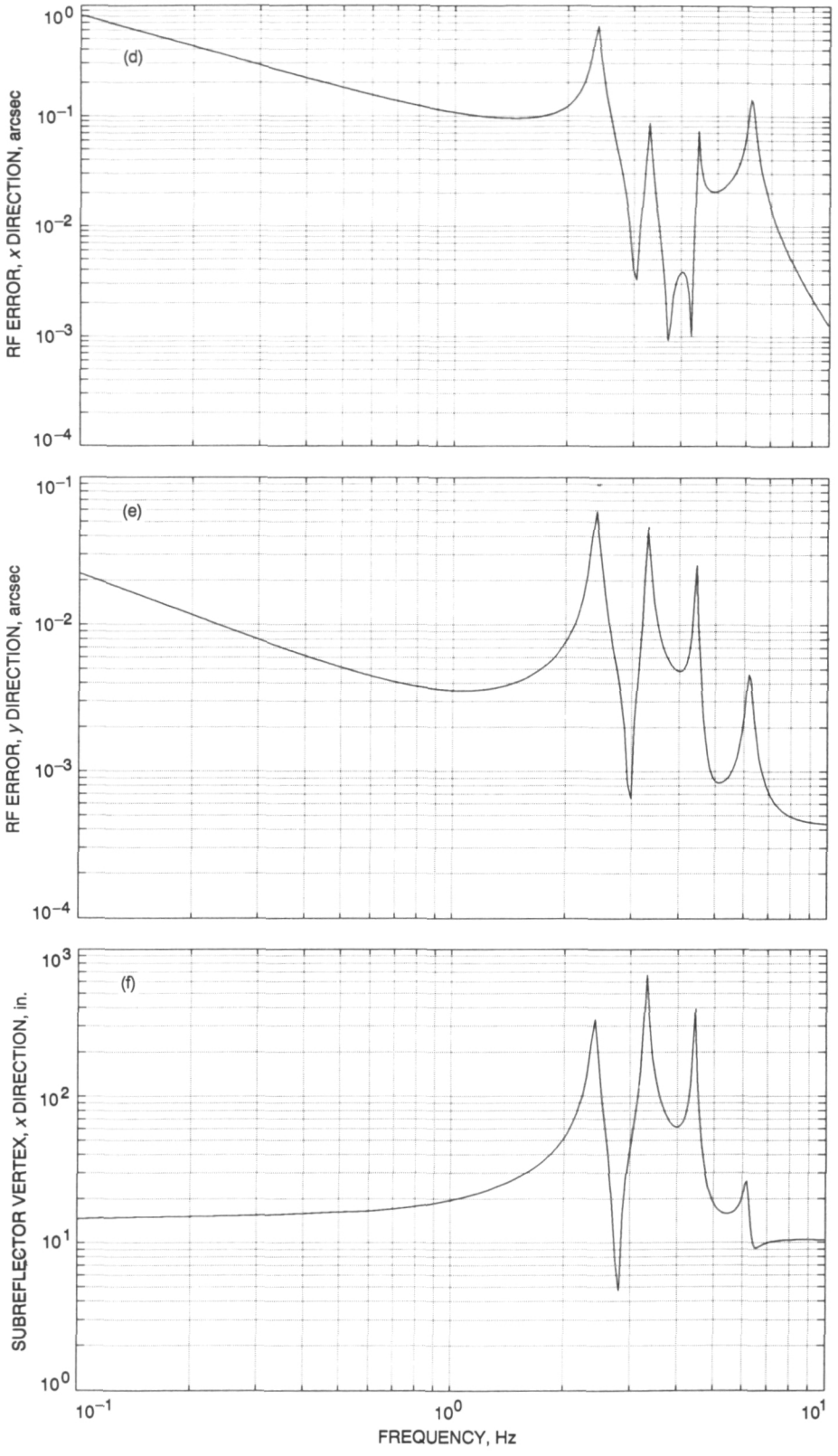
(d)
RF ERROR, x DIRECTION, arcsec
10^0
10^{-1}
10^{-2}
10^{-3}
10^{-4}
(e)
RF ERROR, y DIRECTION, arcsec
10^{-1}
10^{-2}
10^{-3}
10^{-4}
(f)
SUBREFLECTOR VERTEX, x DIRECTION, in.
10^3
10^2
10^1
10^0
10^{-1}
10^0
10^1
FREQUENCY, Hz

Fig. 13 (contd)

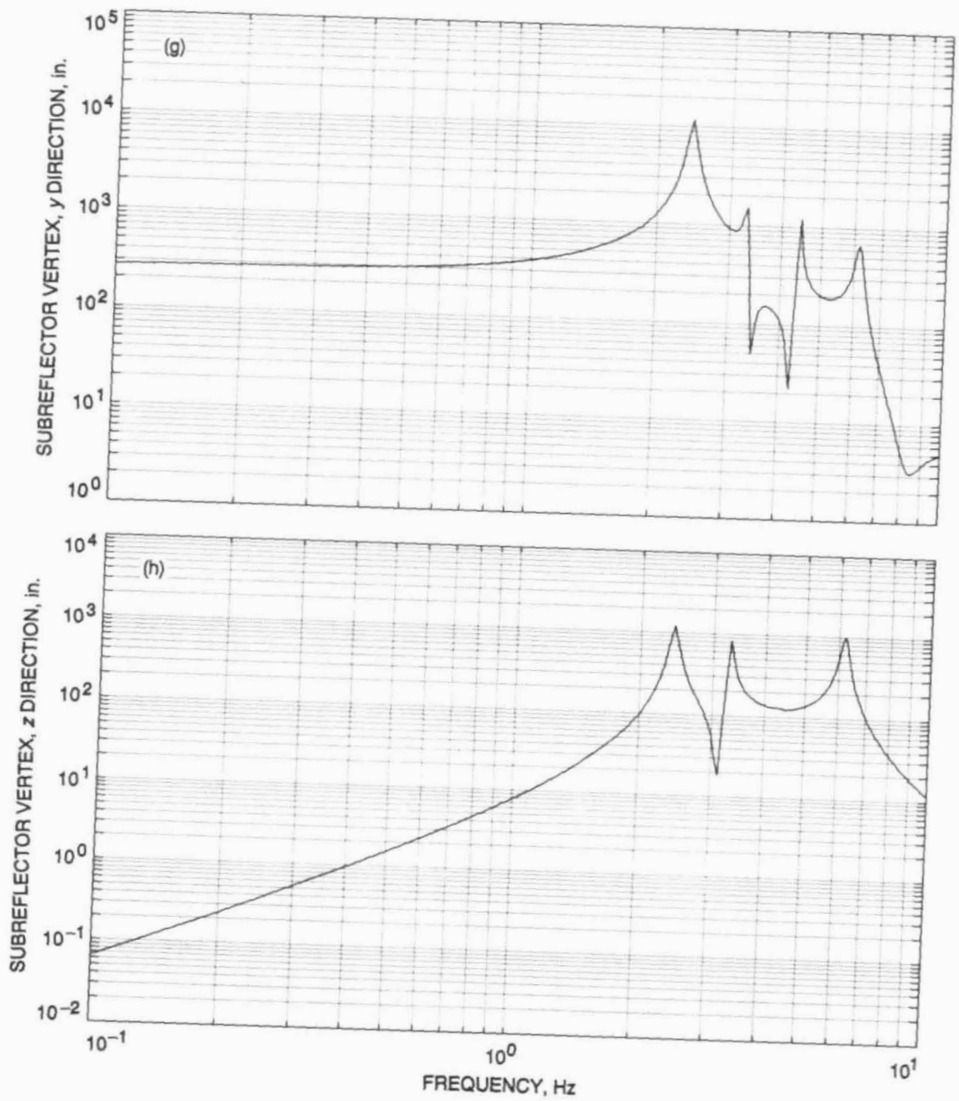
(g)
SUBREFLECTOR VERTEX, y DIRECTION, in.
10^5
10^4
10^3
10^2
10^1
10^0
(h)
SUBREFLECTOR VERTEX, z DIRECTION, in.
10^4
10^3
10^2
10^1
10^0
10^{-1}
10^{-2}
10^{-1}
10^0
10^1
FREQUENCY, Hz

Fig. 13 (contd)

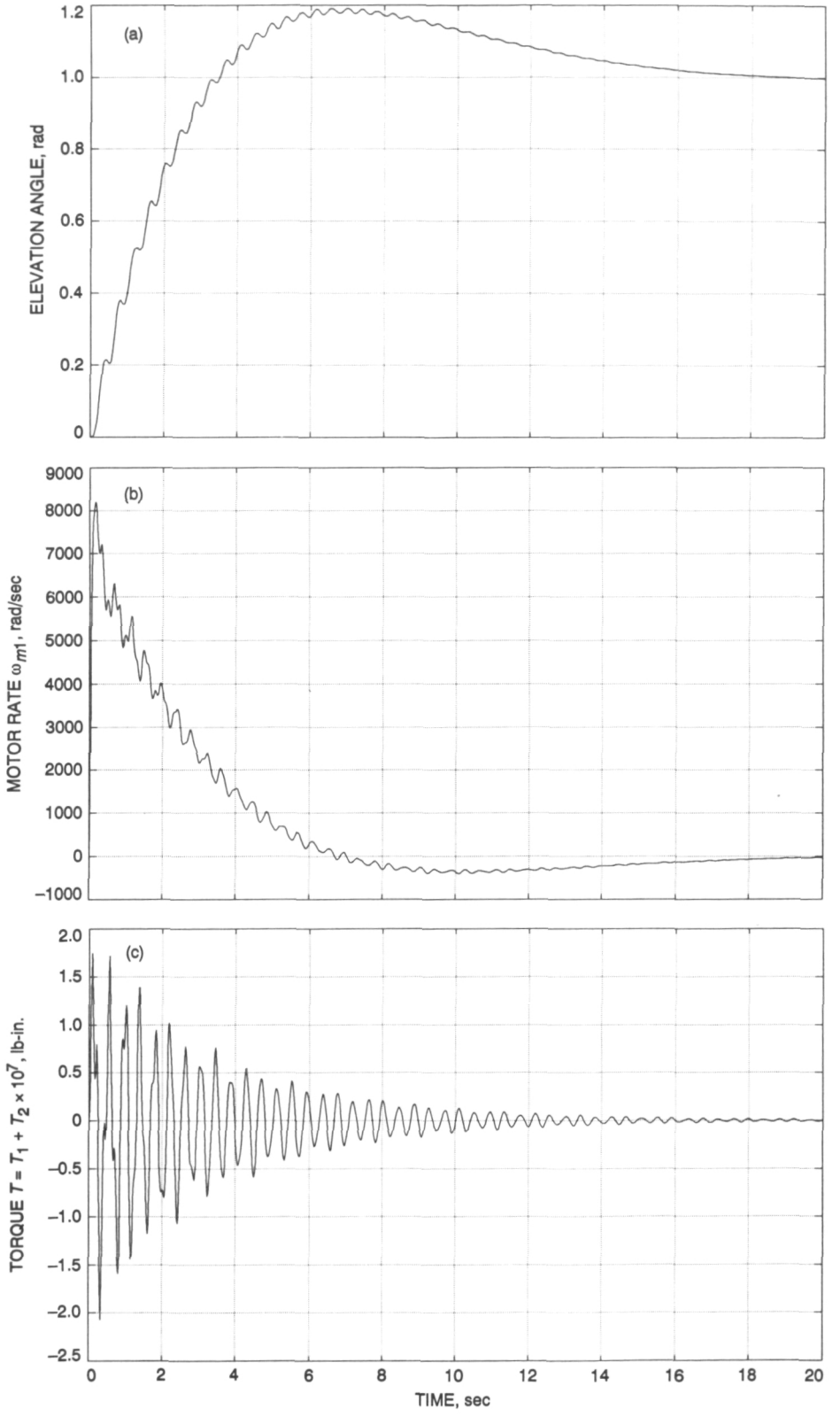

Fig. 14. Step responses for the closed-loop system; position loop closed, $k_{pp} = 0.5$, $k_{ij} = 0.1$; input: elevation angle, rad.

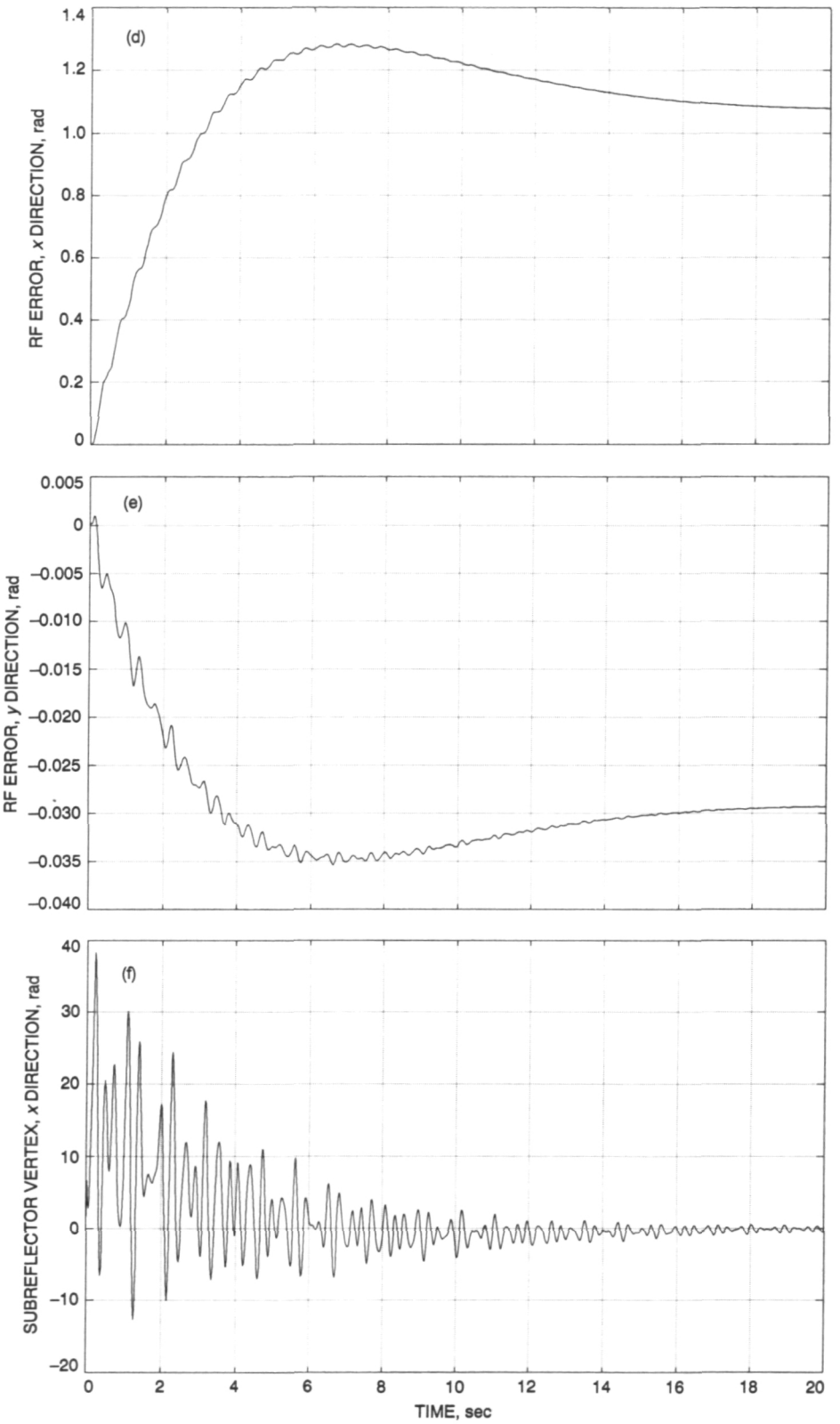
(d)
RF ERROR, x DIRECTION, rad
1.4
1.2
1.0
0.8
0.6
0.4
0.2
0
(e)
RF ERROR, y DIRECTION, rad
0.005
0
−0.005
−0.010
−0.015
−0.020
−0.025
−0.030
−0.035
−0.040
(f)
SUBREFLECTOR VERTEX, x DIRECTION, rad
40
30
20
10
0
−10
−20
0
2
4
6
8
10
12
14
16
18
20
TIME, sec

Fig. 14 (contd)

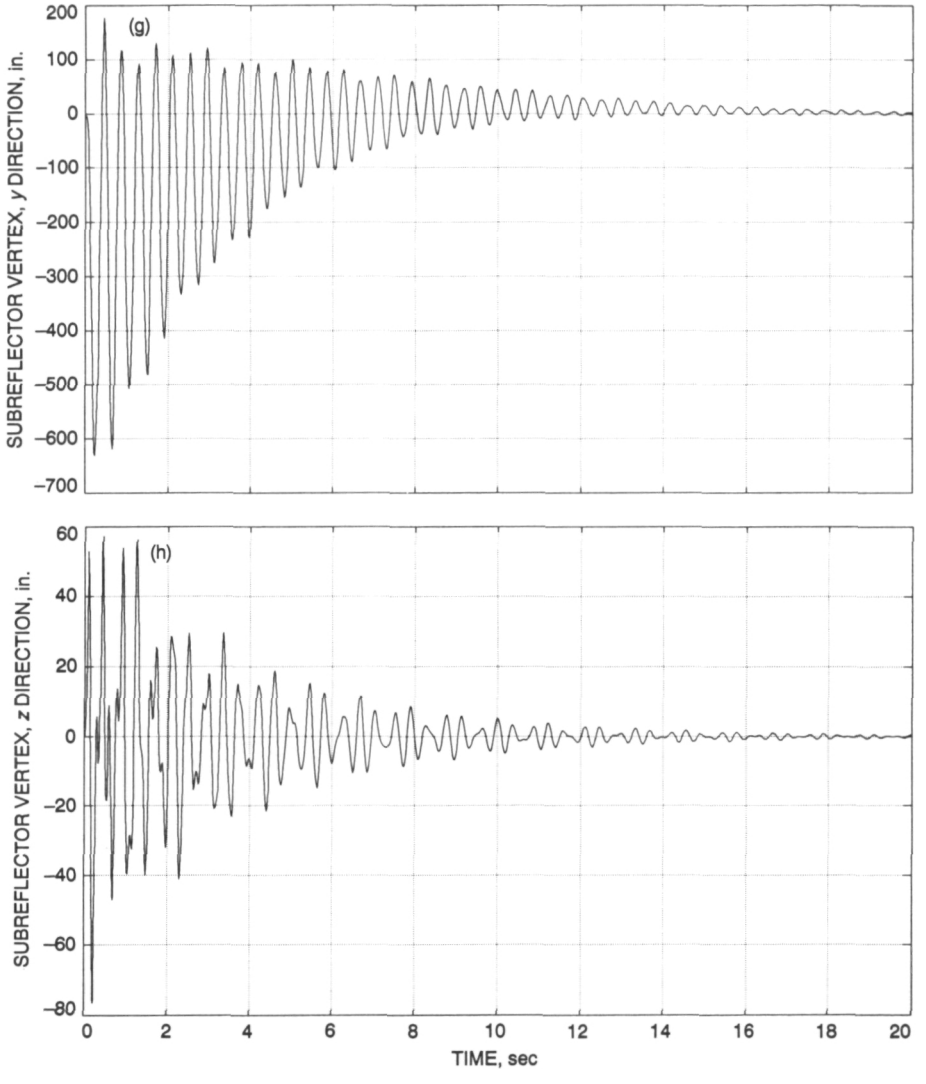
(g)
SUBREFLECTOR VERTEX, y DIRECTION, in.
200
100
0
−100
−200
−300
−400
−500
−600
−700
(h)
SUBREFLECTOR VERTEX, z DIRECTION, in.
60
40
20
0
−20
−40
−60
−80
0
2
4
6
8
10
12
14
16
18
20
TIME, sec

Fig. 14 (contd)

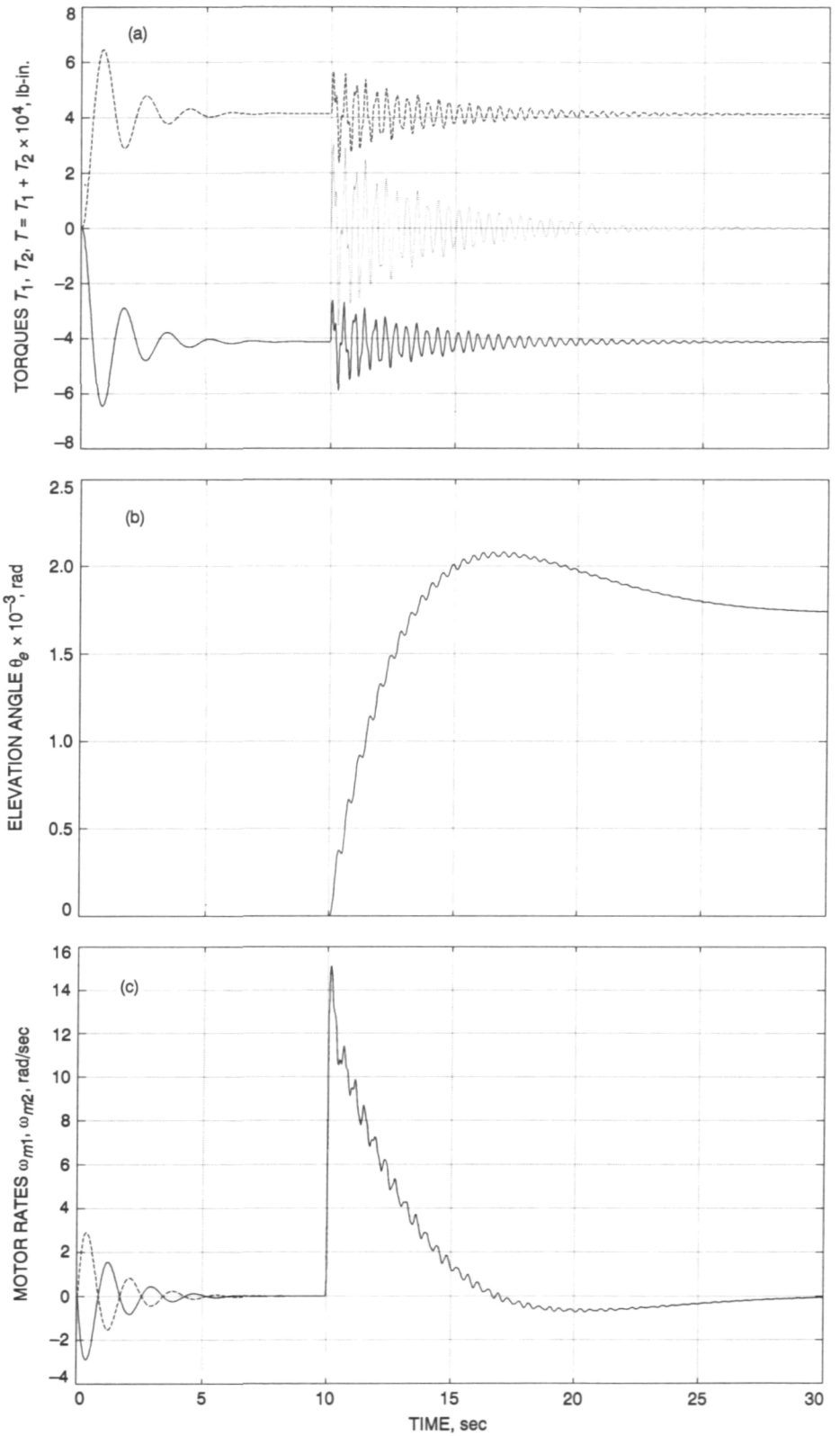

Fig. 15. Step responses of the closed-loop system to the command and bias inputs: step $v_{bias} = 2.5$ V at $t = 0$ and step $\theta_o = 0.1$ deg at $t = 10$ sec.

Appendix A

Parameters of the DSS 13 Antenna

I. Structural Parameters

The structural parameters for the DSS 13 antenna are:

$\alpha =$ 28 deg

$\zeta_i = 0.005,\ i = 1, \ldots, 10$

$\Omega = diag(0,\ 12.4482,\ 12.5833,\ 13.3612,\ 19.7028,\ 20.1747,\ 25.2584,\ 25.8547,\ 27.9621,\ 28.7060)$

$M_m = diag(215.4239,\ 223.8522,\ 38.1610,\ 17.1415,\ 243.8451,\ 58.5778,\ 95.1770,\ 804.4224,\ 18.4959,\ 18.3158)$

Node numbers: $nc = 5380, no = 86302, nu = 86881,$ and $nb = 41212$

Modal matrix: $\Phi = [\phi_1, \phi_2, \ldots, \phi_{10}]$

$\phi_i =$ ith mode shape, ϕ_i

$= [\phi_{i1},\ \phi_{i2},\ \ldots,\ \phi_{i12}]^T$

where:

$\phi_{i1} = ith$ mode component, node nc, x direction

$\phi_{i2} = ith$ mode component, node nc, y direction

$\phi_{i3} = ith$ mode component, node nc, z direction

$\phi_{i4} = ith$ mode component, node no, x direction

$\phi_{i5} = ith$ mode component, node no, y direction

$\phi_{i6} = ith$ mode component, node no, z direction

$\phi_{i7} = ith$ mode component, node nu, x direction

$\phi_{i8} = ith$ mode component, node nu, y direction

$\phi_{i9} = ith$ mode component, node nu, z direction

$\phi_{i10} = ith$ mode component, node nb, x direction

$\phi_{i11} = ith$ mode component, node nb, y direction

$\phi_{i12} = ith$ mode component, node nb, z direction

The modes (in MATLAB notation):

```
phi_1^T = [0.00000012,   -0.00000060,    0.00000003,... % (node nc, x,y,z components)
           0.00000000,    0.17696733,    0.34187825,... % (node no, x,y,z components)
           0.00000000,   -0.00000005,   -0.00000010,... % (node nu, x,y,z components)
           0.00000012,   -0.04215388,    0.00000003];   % (node nb, x,y,z components)

phi_2^T = [0.16089562,   -0.04828905,   -0.01058891,... % (node nc, x,y,z components)
           0.00000000,   -0.00320542,    0.00104308,... % (node no, x,y,z components)
           0.00000000,    0.00012084,    0.00023455,... % (node nu, x,y,z components)
           0.18123627,   -0.05316486,   -0.01040931];   % (node nb, x,y,z components)

phi_3^T = [-0.02516621,  -0.07031944,    0.00690156,... % (node nc, x,y,z components)
            0.00000000,  -0.00103347,    0.00003283,... % (node no, x,y,z components)
            0.00000000,  -0.00024008,   -0.00046601,... % (node nu, x,y,z components)
           -0.02842479,  -0.07567856,    0.00688137];   % (node nb, x,y,z components)

phi_4^T = [0.00351127,    0.03635180,   -0.00294988,... % (node nc, x,y,z components)
           0.00000000,    0.00089782,   -0.00009626,... % (node no, x,y,z components)
           0.00000000,    0.00012046,    0.00023381,... % (node nu, x,y,z components)
           0.00397642,    0.03904565,   -0.00295351];   % (node nb, x,y,z components)

phi_5^T = [0.01726125,    0.21422039,   -0.02128878,... % (node nc, x,y,z components)
           0.00000000,    0.41745298,   -0.03668607,... % (node no, x,y,z components)
           0.00000000,    0.01317732,    0.02557758,... % (node nu, x,y,z components)
           0.01343854,    0.25263344,   -0.02139128];   % (node nb, x,y,z components)
```

$$
\begin{array}{lrrll}
\phi_6^T = & [0.08392051, & 0.00028101, & -0.03029582,\ldots & \% \text{ (node } nc,\ x,y,z \text{ components)} \\
& 0.00000000, & -0.00560731, & -0.00120284,\ldots & \% \text{ (node } no,\ x,y,z \text{ components)} \\
& 0.00000000, & -0.00020205, & -0.00039219,\ldots & \% \text{ (node } nu,\ x,y,z \text{ components)} \\
& 0.08607231, & -0.00154962, & -0.03083227]; & \% \text{ (node } nb,\ x,y,z \text{ components)} \\
\phi_7^T = & [-0.02218441, & 0.16344080, & -0.01364561,\ldots & \% \text{ (node } nc,\ x,y,z \text{ components)} \\
& 0.00000000, & -0.02133899, & 0.00544590,\ldots & \% \text{ (node } no,\ x,y,z \text{ components)} \\
& 0.00000000, & 0.00065982, & 0.00128072,\ldots & \% \text{ (node } nu,\ x,y,z \text{ components)} \\
& [-0.01743287, & 0.15653900, & -0.01357982]; & \% \text{ (node } nb,\ x,y,z \text{ components)} \\
\phi_8^T = & [-0.30854177, & 0.04674442, & 0.18580163,\ldots & \% \text{ (node } nc,\ x,y,z \text{ components)} \\
& 0.00000000, & 0.14007292, & 0.79574209,\ldots & \% \text{ (node } no,\ x,y,z \text{ components)} \\
& 0.00000000, & 0.05702746, & 0.11069132,\ldots & \% \text{ (node } nu,\ x,y,z \text{ components)} \\
& [-0.23322315, & 0.05969981, & 0.18902462]; & \% \text{ (node } nb,\ x,y,z \text{ components)} \\
\phi_9^T = & [-0.00970566, & -0.01171182, & 0.00170980,\ldots & \% \text{ (node } nc,\ x,y,z \text{ components)} \\
& 0.00000000, & -0.02275614, & 0.02106441,\ldots & \% \text{ (node } no,\ x,y,z \text{ components)} \\
& 0.00000000, & -0.00178816, & -0.00347085,\ldots & \% \text{ (node } nu,\ x,y,z \text{ components)} \\
& [-0.01092381, & -0.01958129, & 0.00171795]; & \% \text{ (node } nb,\ x,y,z \text{ components)} \\
\phi_{10}^T = & [-0.05660426, & 0.01088616, & 0.01266761,\ldots & \% \text{ (node } nc,\ x,y,z \text{ components)} \\
& 0.00000000, & 0.00316858, & 0.00525204,\ldots & \% \text{ (node } no,\ x,y,z \text{ components)} \\
& 0.00000000, & 0.00090903, & 0.00176443,\ldots & \% \text{ (node } nu,\ x,y,z \text{ components)} \\
& -0.05696018, & 0.00916372, & 0.01287218]. & \% \text{ (node } nb,\ x,y,z \text{ components)}
\end{array}
$$

II. Rate-Loop System Parameters

The rate-loop system parameters for the DSS 13 antenna are:

$k_1 = 716.197$ V sec/rad

$k_m = 15.72$ lb/A

$k_b = 1.79$ V sec/rad

$k_s = 0.8$ V/V

$k_{tach} = 0.0384123$ V sec/rad

$k_r = 80$ V/sec V, range: $49 - 83$

$k_i = 87.13$ V/sec V

$k_{ii} = 0.1$

$k_{pp} = 0.5$

$k_{cur} = 0.12658$ V/A

$k_f = 54$ V/V

$k_{go} = 1.5 \times 10^7$ lb/rad

$k_{ctfr} = 0.33$

$k_{ct} = 0.11111$

$k_{bs} = 0.66$

$\tau_1 = 0.0063662$ sec

$\tau_2 = 0.094$ sec

$\tau_3 = 0.002$ sec

$\tau_4 = 0.00484$ sec

$\tau_5 = 0.0021$ sec

$\tau_6 = 0.7304$ sec

$N = 354$

$J_m = 1.236$ lb/sec^2

$R_a = 0.456\ \Omega$

$L_a = 0.011\ H$

Appendix B

From the Finite-Element Model to the State-Space Model

The state-space model of a flexible structure is obtained from its finite-element model, which consists of the mass M $(m \times m)$, stiffness K $(m \times m)$, input B_o $(m \times s)$, output C_{oq} $(r \times m)$, C_{ov} $(r \times m)$ matrices, the input $u(t)$ $(s \times 1)$, and output $y(t)$ $(r \times 1)$. The input–output relationship is given by the second-order differential equation

$$M\ddot{q} + Kq = B_o u, \quad y = C_{oq}q + C_{ov}\dot{q} \tag{B-1}$$

where q is the vector of structural displacements.

Consider now a modal matrix Φ $(m \times p)$, $p \leq m$, which consists of p eigenvectors ϕ_i (mode shapes), $i = 1, \ldots, p$:

$$\Phi = [\phi_i, \phi_2, \ldots, \phi_p] \tag{B-2}$$

which diagonalize M and K:

$$M_m = \Phi^T M \Phi, \quad K_m = \Phi^T K \Phi \tag{B-3}$$

i.e., M_m and K_m are diagonal $(p \times p)$ matrices of modal mass and stiffness. When a new variable q_m $(p \times 1)$ is introduced such that

$$q = \Phi q_m \tag{B-4}$$

and left-multiplying Eq. (B-1) by Φ^T, one obtains either

$$\Phi^T M \Phi \ddot{q}_m + \Phi^T K \Phi q_m = \Phi^T B_o u, \qquad y = C_{oq}\Phi q_m + C_{ov}\Phi\dot{q}_m \tag{B-5a}$$

or

$$M_m \ddot{q}_m + K_m q_m = \Phi^T B_o u, \quad y = C_{oq}\Phi q_m + C_{ov}\Phi\dot{q}_m \tag{B-5b}$$

or

$$\ddot{q}_m + M_m^{-1} K_m q_m = M_m^{-1}\Phi^T B_o u, \qquad y = C_{oq}\Phi q_m + C_{ov}\Phi\dot{q}_m \tag{B-5c}$$

Denote $M_m^{-1}K_m = \Omega^2$, where Ω is a diagonal $(p \times p)$ matrix of natural frequencies (rad/sec). At this stage a damping matrix Z is introduced, $Z = diag(\zeta_i)$, $i = 1, \ldots, p$, such that $2Z\Omega = M_m^{-1}D_m$, and D_m is a modal damping matrix (assumed to be known), so that from Eq. (B-5c) the modal model is acquired:

$$\ddot{q}_m + 2Z\Omega\dot{q}_m + \Omega^2 q_m = M_m^{-1}\Phi^T B_o u, \qquad y = C_{oq}\Phi q_m + C_{ov}\Phi\dot{q}_m \tag{B-6}$$

Define a state variable x

$$x = \begin{bmatrix} x_1 \\ x_2 \end{bmatrix} = \begin{bmatrix} q_m \\ \dot{q}_m \end{bmatrix} \tag{B-7}$$

then, Eq. (B-6) can be presented as a set of first-order equations:

$$\dot{x}_1 = x_2$$

$$\dot{x}_2 = -\Omega^2 x_1 - 2Z\Omega x_2 + M_m^{-1}\Phi B_o u$$

$$y = C_{oq}\Phi x_1 + C_{ov}\phi x_2$$

or in the following form

$$\dot{x} = Ax + Bu, \quad y = Cx \tag{B-8a}$$

where

$$A = \begin{bmatrix} 0 & I \\ -\Omega^2 & -2Z\Omega \end{bmatrix}, \quad B = \begin{bmatrix} 0 \\ M_m^{-1}\Phi^T B_o \end{bmatrix}, \qquad C = [C_{oq}\Phi \;\; C_{ov}\Phi] \tag{B-8b}$$

is the sought state-space model in modal coordinates.

Appendix C

A Balanced Representation of a Linear System

Consider a stable, linear, time-invariant system:

$$\dot{x} = Ax + Bu, \quad y = Cx, \quad x(0) = x_o \tag{C-1}$$

where $x \in R^n$ is the system state, $u \in R^p$ is the system input, $y \in R^m$ is the system output, and (A, B, C) is the system state-space representation. The system controllability and observability grammians W_c and W_o are solutions of the Lyapunov equations

$$AW_c + W_cA^T + BB^T = 0, \quad A^TW_o + W_oA + CC^T = 0 \tag{C-2}$$

The system representation is balanced if its controllability and observability grammians are diagonal and equal. Hence, for the balanced representation $(A_b, B_b, C_b) = (T^{-1}AT, T^{-1}B, CT)$, the following is true:

$$W_c = W_o = \Gamma^2,$$

$$\Gamma = diag(\gamma_1, \ldots, \gamma_n), \quad \gamma_i \geq o, \quad i = 1, \ldots, n \tag{C-3}$$

where T is a linear transformation and γ_i is the ith Hankel singular value of the system.

The transformation T is determined as follows:

$$T = PU\Gamma^{-1}, \quad T^{-1} = \Gamma^{-1}V^TQ \tag{C-4}$$

The matrices Γ, V, and U are obtained from the singular value decomposition of the matrix H:

$$H = V\Gamma^2U^T \tag{C-5}$$

where $H = QP$, and P and Q form the following decomposition of grammians:

$$W_c = PP^T, \quad W_o = Q^TQ \tag{C-6}$$

for example, Cholesky, or singular-value decomposition.